Ore Geology Reviews 104 (2019) 707–721

Contents lists available at ScienceDirect

Ore Geology Reviews

journal homepage: www.elsevier.com/locate/oregeorev

Petrogenesis of Mesozoic granitoids and genesis of Au–polymetallic mineralization in the Sonchon district, DPR Korea

Ung–Ho Pak*, Chang–Guk Jon, Chung–Nam O, Kwang–U Choe

Faculty of Geology, Kim Il Sung University, Ryongnam–Dong, Taesong District, Pyongyang, Democratic People's Republic of Korea

ARTICLE INFO

Keywords:
Diorite
Granodiorite
Biotite granite
Fluid inclusions
REE
Sulfur isotope
Sonchon

ABSTRACT

The Au–polymetallic deposit in the Sonchon district is located in the western parts of North Pyongan Province, DPR Korea. Here, we present a detailed study of the petrogenesis, magma source of the Mesozoic granitoids, and the sources of ore–forming materials and fluids. Mesozoic granitoids consist of diorite, granodiorite and biotite granite. These rocks are alkali–enriched (K_2O + Na_2O = 5.02–7.75 wt%) and classified as high–K calc–alkaline. The diorite is metaluminous, while the granodiorite and biotite granite are weakly peraluminous and peraluminous, respectively. The samples show high CaO/Na_2O ratios of 1.66–2.16 for the diorite and 0.74–1.35 for the granodiorite, indicating a derivation from clay–poor psammite–derived melt source, and the biotite granite has low CaO/Na_2O ratios of 0.14–0.38, indicating a derivation from clay–rich pelite–derived melt source. The biotite granite belongs to fractionated M–, I–, and S–type granites (FG), whereas the granodiorite and the diorite belong to unfractionated M–, I–, and S–type granites (OGT). These rocks are typically arc-related. The similar REE distribution patterns of these rocks show that they are relatively uniform with partial melting processes playing an important role in their generation. The REE distribution patterns of ore–bearing quartz are similar to those of granodiorite rather than diorite, biotite granite and wall rocks, suggesting that they were mainly inherited from the granodiorite. The barren quartz has more negative Eu anomalies than the ore–bearing quartz. The histogram of sulfur isotopic composition shows that the $\delta^{34}S$ values are mainly distributed around +5 to +10‰ and indicate the sulfur within sulfide was derived from a magmatic source. The absence of sulfates in ore bodies indicates that the low fO_2 and high pH of ore–forming fluid system. Fluid inclusions in quartz have only aqueous–gas phases without CO_2–rich phase and daughter minerals, indicating that ore–forming fluids was homogenous magmatic and had low salinity. According to the values of X (Na^+)/X (K^+) ratios, X (Na^+)/X (Ca^{2+} + Mg^{2+}) ratios, and X (F^-)/X (Cl^-) ratios, the ore–forming fluids could be interpreted as a mixture of magmatic and meteoric water. Microthermometric analyses indicate that these inclusions have medium temperature (223.5–286.3 °C) and low salinity (1.39–4.01 wt% NaCl) and are NaCl + H_2O or NaCl + KF + H_2O systems. All these data in this study suggest that the Sonchon Au–polymetallic deposit is mesothermal and related to the granodiorite.

1. Introduction

The Au–polymetallic deposit in the Sonchon district is an important economic producer of Au, Ag, Pb and Zn minerals in DPR Korea. Because there are Neoarchean Rangnim Metamorphic Belt, Neoarchean Ryonhwasan Complex (granitoid), Paleozoic Namgang Complex (gabbro–diabase), Mesozoic Tanchon Complex (granitoid) and numerous faults in this district, there is no consensus of opinion about the genesis of the deposit yet. Some researchers believe that the deposit was formed by metamorphic fluids derived during metamorphism of Rangnim formation in the Neoarchean era. They have the opinion that Rangnim formation with high metamorphic grade is exposed in the ore district and its original rocks were composed of hydromica, montmorillonite and sandy clay with Fe–Mg–Al silicates. Moreover, in their opinion, the Mesozoic granitoids are not associated with gold mineralization because they are S–type and are exposed as small scale for mineralization, and the alteration associated with the mineralization is characterized by chloritization and sericitization developed during retrogressive metamorphism (Li, 1998, 2009). Other researchers argued that the Sonchon mineralization is magmatic hydrothermal associated with Mesozoic granodiorite and biotite granite because the ore bodies are distributed in a 6 km range around these granitoids and located mainly along NE–trending faults formed in late Paleozoic and early Mesozoic. The latter researchers suggested that the Mesozoic granitoids belong to

* Corresponding author.
E-mail address: ryongnam28@yahoo.com (P. Ung–Ho).

https://doi.org/10.1016/j.oregeorev.2018.12.004
Received 16 June 2018; Received in revised form 23 November 2018; Accepted 10 December 2018
Available online 11 December 2018
0169-1368/

I or I–S–types and can be associated with gold mineralization (Choe et al., 2011; Paek et al., 1993). In the Sonchon district, the detailed research on Mesozoic granitoids and Neoarchean granitoids of major and trace elements, sulfur isotope and fluid inclusions in minerals which are important to understand ore genesis, were less studied. The petrochemical signatures of the granitoids record important information on magma sources and their nature (Barbarin, 1999; Zhu et al., 2013) and the characteristics of ore–forming fluids provide important clues for understanding the genesis of ore deposits. Gold deposits are generally formed as a consequence of tectonic, geological and geochemical conditions (Groves and Santosh, 2015), in which the nature of the hydrothermal fluids is of fundamental importance (Chen et al., 2007). Therefore, an accurate assessment of the nature and composition of the mineralizing fluids is a key to understanding the origin of hydrothermal deposits.

In this paper, we discuss analytical results of major, trace elements and REEs of the Mesozoic granitoids, Neoarchean granitoids and the ore bodies, and S isotope compositions of sulfide minerals, fluid inclusion compositions and microthermometric measurements of ore–bearing quartz in the Sonchon deposit. We discuss the magma sources of the Mesozoic granitoids and its relationship with Au–polymetallic deposit, and the sources of ore–forming materials and fluids.

2. Deposit geology

The Sonchon district is located on the southwestern parts of the Rangnim Massif, Sino–Korean Craton (Fig. 1a), and comprises Neoarchean Songwon and Rangnim metamorphic belts and the Proterozoic Jikhyon group. Main faults are NE–SW–trending (Fig. 1b). The intrusive rocks exposed in this district are Neoarchean granitoids, Proterozoic Syenite and Mesozoic Jurassic granitoids.

The Sonchon deposit is located on the central part of this district (Fig. 1b). It consists of 6 ore bodies; Wolchon, Paekhyon, Somokgol, Dohua, Ryongsu, and Songrim (Fig. 2).

The stratigraphic sequence in the mining district consists of Neoarchean metamorphic rocks (Rangnim Metamorphic Belt) and Quaternary. The Neoarchean metamorphic rocks are scattered throughout the Neoarchean granitoids as irregular xenoliths. Main rocks are biotite gneiss, graphite–bearing gneiss, quartzitic gneiss and migmatite.

The study area does not have a sedimentary cover, and the Neoarchean Rangnim Metamorphic Belt is spread from place to place as xenoliths and it was strongly migmatized. Therefore, the folds cannot be observed in this area.

The Sonchon district has five fault zones; i.e., NE–SW–trending Sonchon, Paekhyon, and Pudong faults, which were formed in late Paleozoic and early Mesozoic era crosscutting the Neoarchean Rangnim Metamorphic Belt and the Paleozoic Namgang Complex in the north parts of the deposit. The NE–SW–trending Songhyon–Zanggong and EW–trending Sonchon–Indu faults were formed at late Mesozoic era. The NE–SW–trending faults (Sonchon, Paekhyon, and Pudong) are reversed strike–slip faults, moving the north block to a NW trend. These faults generally trend northeast, dip 70°–80° to the southeast, extend to the northeast–southwest with lengths of 18 km and widths of about 50 m, and were intruded by dykes of plagioclase–porphyrite, quartz–orthophyre and felsite. These faults were repeatedly reactivated and at that time formed numerous NS–, NE– and EW–trending subsidiary faults. These subsidiary faults crosscut the NE–SW–trending faults or run subparallel to them. The ore bodies are located in these faults with lengths of 120–700 m and widths of 0.03–0.8 m. The NE–SW–trending Songhyon–Zanggong fault trends northeast, dips 30° to the southeast and crosscuts the Mesozoic granodiorite. The EW–trending fault is a normal fault extended to east–west with length of 35 km, width of 10 m and crosscuts all NE–SW–trending faults, and has no relationship with gold mineralization (Fig. 2).

The intrusive rocks exposed in the study area are Neoarchean

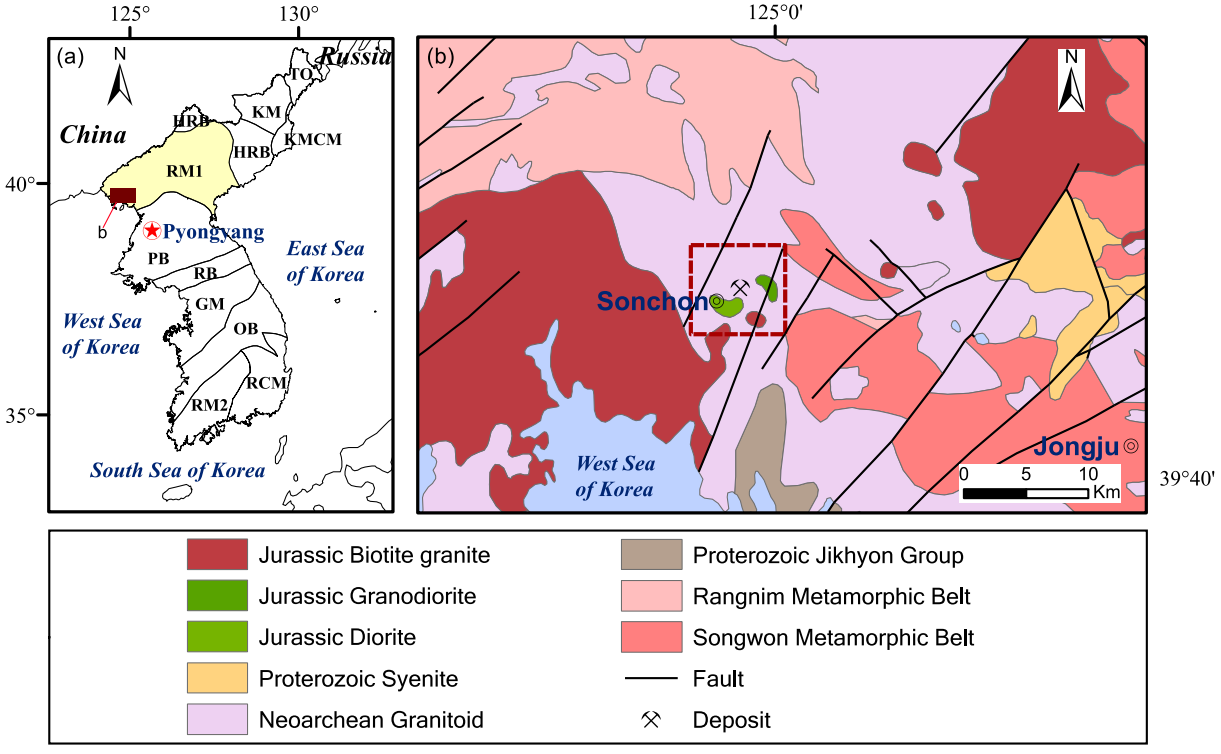

Fig. 1. Simplified regional geological map of the Sonchon district in DPR Korea. The red box indicates the area shown in Fig. 2. TO, Tumangang orogen; KM, Kwanmo massif; HRB, Hyesan–Riwon basin; KMCM, Kilju–Myongchon continental margin; RM1, Rangnim massif; PB, Pyongnam basin; RB, Rimjingang Belt; GM, Gyonggi massif; OB, Okchon basin; RM2, Ryongnam massif; RCM, Rakdonggang continental margin. (For interpretation of the references to color in this figure legend, the reader is referred to the web version of this article.)

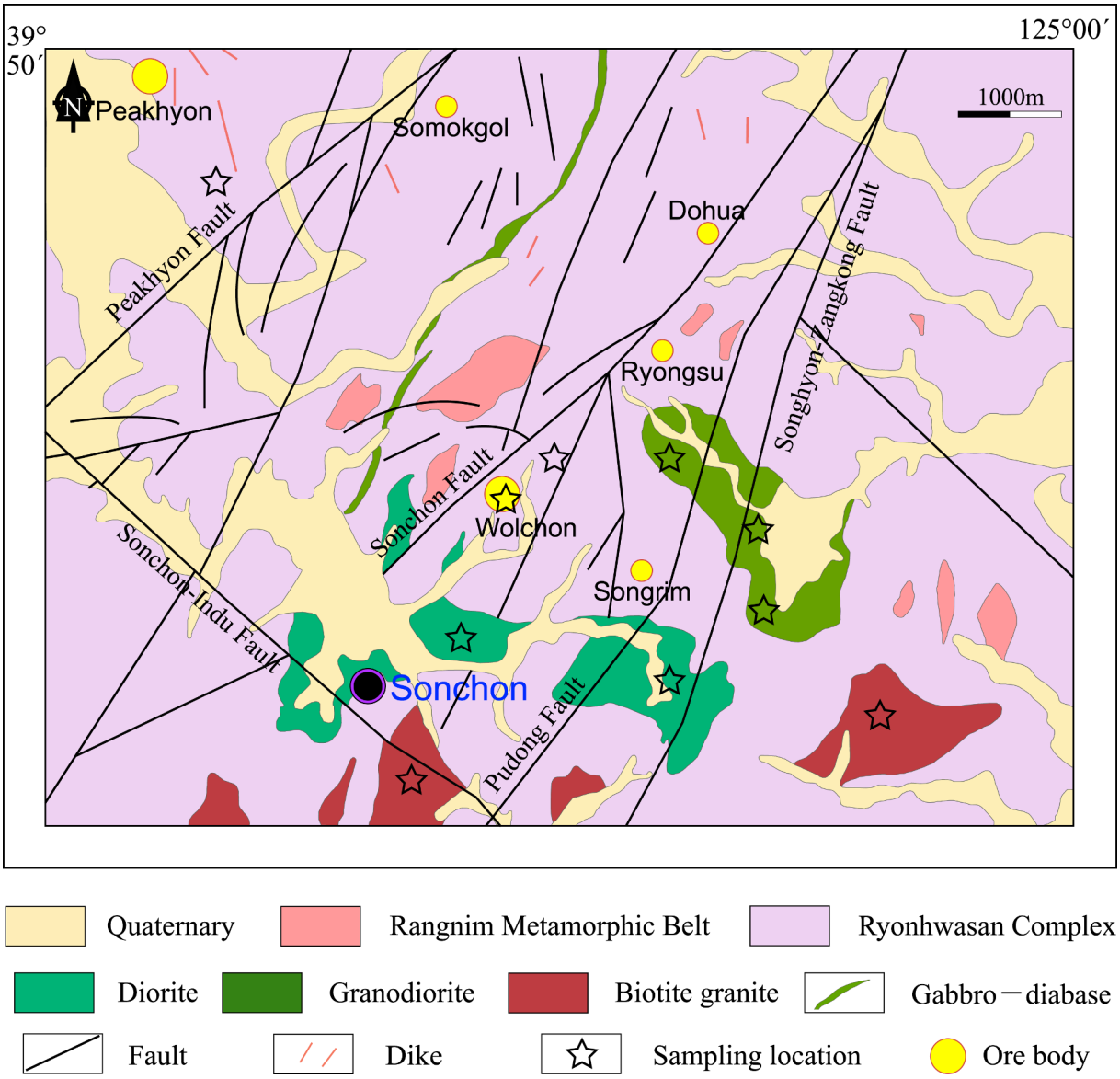

Fig. 2. Detailed geological map of the Sonchon deposit.

Ryonhwasan Complex, Paleozoic Namgang Complex, and Mesozoic Tanchon Complex.

The Neoarchean Ryonhwasan Complex is divided into three groups taking into account its petrographic and petrochemical signature. The first and third groups are exposed in the study area. The first group is widely distributed in the area, whereas the third group is scattered only in the northwest of the area. The first group consists of medium to coarse–grained porphyritic biotite granite, gneissose granite and fine–grained porphyritic granite with pale gray color. The main minerals are quartz (5–30%), albite (20–40%), microcline (5–35%) and biotite (3–10%), and accessory minerals are garnet, cordierite, graphite, apatite, zircon, titanite and monazite. Muscovite, sericite, chlorite and talc are secondary minerals. All ore bodies are hosted in these granitoid (Fig. 2). The third group is divided into the fine to medium–grained alaskite, biotite alaskite and biotite granite on the basis of structural, petrographic and petrochemical characteristics. These rocks are composed of quartz (30%), plagioclase (14–50%), K–feldspar (10–50%), biotite (3–10%) as main minerals and zircon, garnet, titanite as accessory minerals. The secondary minerals are epidote and sericite. The ages of Neoarchean Ryonhwasan Complex obtained by zircon U–Pb ICP-MS dating are 2497–2300 Ma (Han and Kim, 2005).

The Paleozoic Namgang Complex (gabbro and diabase) occurs in the first group of the Neoarchean granitoid as long cross–cutting dikes or veins with E–trending dip and NE–trending strike and crosscut by the Mesozoic diorite (Fig. 2). The gabbro–diabase is massive with dark gray and gray–green color. The main minerals are plagioclase (40–50%), pyroxene (30–40%), hornblende (10–20%) and quartz (5–10%), and accessory minerals are zircon and sphene. Epidote, zoisite, sericite and chlorite are secondary minerals. In the gabbro–diabase are disseminated pyrite, marcasite and minor chalcopyrite.

The Mesozoic Tanchon Complex is divided into three intrusive phases, most of which consist of the second phase (biotite granite), and partly of fine–grained alaskites of the third phase, while first phase is rare (Paek et al., 1993). In the study area, they are represented by first and second phases (Fig. 2). The first phase is exposed in the southern and southeastern parts of the area with 3–4 km^2 as two intrusive (diorite and granodiorite) and consists of diorite, granodiorite, quartz diorite and gabbro diorite. These rocks have fine to medium–grained texture and massive structure with dark gray–green color and are characterized by the presence of plagioclase (40–50%), pyroxene (10–20%), hornblende (5–10%), biotite (5–10%), minor amounts of quartz and K–feldspar as the main minerals. Accessory minerals include

zircon, monazite, ilmenite, apatite and secondary minerals are sericite, chlorite, epidote and zoisite. In the inner parts of the granodiorite Sn-W mineralization are present. The second phase (biotite granite) is exposed in the southwestern and western parts of the district and consists of coarse–grained porphyritic biotite granite, porphyritic hornblende–biotite granite, medium–grained biotite granite, fine–grained porphyritic biotite granite and granodiorite. These rocks have fine to medium–grained texture with dark green color. The main minerals are plagioclase (30–35%), K–feldspar (30–35%), quartz (25%), biotite (4–5%) and the accessory minerals contain zircon, apatite, monazite and ilmenite. The secondary minerals are sericite, chlorite, kaolinite and epidote. The geological age of Tanchon Complex is 190 Ma by the Rb–Sr method and 112 Ma by the K–Ar method (Paek et al., 1993).

The ore bodies are distributed in the northeast of the deposit and concentrated around the Mesozoic Tanchon Complex becoming less common away from it. In the study area, the main ore bodies are Wolchon, Paekhyon, Somokgol, Dohua, Ryongsu, and Songrim. The Wolchon and Paekhyon ore bodies play important roles in the production of gold. All ore bodies are hosted in Neoarchean Ryonhwasan Complex (granitoid).

The Wolchon ore body is quartz–sulfide vein with minor content native gold. The ore minerals are pyrite, galena, arsenopyrite and minor sphalerite, and pyrite is the most abundant sulfide. The ore minerals are predominantly distributed as sparse disseminations or as dense disseminations in quartz with massive, veinlets and vuggy structures (Fig. 4e), and gold is mainly contained in pyrite and galena. Although pyrite, sphalerite and arsenopyrite are predominantly euhedral or subhedral, some display anhedral with brecciated textures. Galena occurs as anhedral grains between pyrite and sphalerite (Fig. 4e–f). Quartz and chalcedony quartz are the most abundant gangue minerals with fine–grained bladed texture and occur as massive, brecciated, vuggy structures. The gold grades range from 1.33 g/t to 25 g/t. The nature of Dohua, Ryongsu and Songrim ore bodies is similar to that of Wolchon.

The Paekhyon and Somokgol ore bodies are quartz vein–style with a few sulfides. The Au and Ag grades show a negative correlation with one another. The content of gold (average, 4.7 g/t) is lower than the content of silver (average, 400 g/t). The average grades of gold increase from shallow levels (23.5 g/t) to deeper levels (161 g/t). The main ore minerals are pyrite, native gold, sphalerite, galena, native silver, electrum, argentite, pearceite, chalcopyrite, arsenopyrite and pyrrhotite. In general, in the deposit district the Au grade increases away from the Mesozoic granitoids, whereas the Ag grade decreases.

Most researchers believe that the ore bodies formed in four stages (Choe et al., 2011). Stage 1 is represented by alkaline metasomatism with weak gold mineralization (0.3–0.5 g/t) and low–sulfidation. Stage 2 is barren white quartz vein–style with weak gold and sulfide mineralization (0.1–0.2 g/t of gold). Stage 3 is the most important stage of gold mineralization, which is characterized by high content of gold (164.7–204.3 g/t) and ore–bearing white–gray quartz vein with sulfide such as pyrite, sphalerite and galena (Fig. 4c). According to the crystallization order of sulfides, this stage is subdivided into the sphalerite and galena substages. Sphalerite crystallized early with white or gray–white quartz, pyrite, arsenopyrite and native gold. The open spaces between shattered sphalerite grains are filled by galena formed in later substages with dark gray or gray–white quartz and argentite. Stage 4 is characterized by barren calcite vein with very weak gold and sulfide mineralization (Fig. 4d).

The alteration of wall rock associated with gold mineralization consists of chloritization, silicification and sericitization (Fig. 3c–d). The chloritization develops in the brecciated wall rock or gradually in the ore bodies, which is accompanied by the sericitization, forming the chlorite–sericite alteration zone with increasing content of silver. Along the contact of the ore body with wall rocks are often observed lamprophyre veins (Fig. 3b). Where fine–grained pyrite is disseminated in this alteration zone, the grade of gold and silver is increased. Silicification occurs not only in wall–rocks with quartz veins and chalcedony quartz, but in contact between the wall–rock and granitoids (Fig. 3a and b). This alteration was developed in the early and main stages of mineralization, and often occurs in Paekhyon, Dohua, Somokgol ore bodies. On the basis of Pb isotope composition of galena in the Wolchon ore body, the age varies from 163 to 170 Ma (Choe et al., 2011).

3. Sample preparations and analytical methods

3.1. Major and trace element analyses

Fresh samples–including diorite (3), granodiorite (6) and biotite granite (4) were collected from the study area and the ore–bearing quartz (2) and barren quartz (2) were chosen from stage 3 vein (level 7) and stage 2 vein (level 7) in the Wolchon ore body, repectively. The number in brackets is the number of samples. Samples were crushed into small grains (0.3–0.5 mm), handpicked under a binocular microscope to remove visible impurities, ultrasonically cleaned in distilled water and dried. The samples were ground in agate mortar and the resulting powder was used for analyses of major and trace elements. Major element analysis was carried out using X–ray fluorescence (XRF) spectrometer with 0.1 wt% detection limits at the Analytical Institute of our University. Loss on ignition (LOI) is the weight difference between burning and very high temperature heating. Trace elements and REEs were analyzed using inductively coupled plasma–mass spectrometry (ICP–MS) with detection limits 0.01–0.1 ppm at the Sukchon Analytical Institute in South of Pyongan Province. The rare earth elements analysis was carried out for diorite (2), granodiorite (2), biotite granite (2), wall rocks (2), ore–bearing (2) and barren quartz (2).

3.2. S isotopes of sulfides

S isotopic analyses were performed on pyrite (12), galena (2) and sphalerite (5) from the Wolchon ore body (level 7). The samples were crushed to 0.1–0.3 mm and cleaned. The pure sulfide minerals were handpicked under a binocular microscope and were converted to SO_2 by heating to 1200 °C in a stream of oxygen, and then the SO_2 samples were analyzed directly using a MAT–251EM mass spectrometer at the Sukchon Analytical Institute. Isotope data are reported in the conventional δ notation relative to the CDT standard. The standard error of each analysis is about ± 0.3‰.

3.3. Fluid inclusions

For petrology and microthermometric studies of fluid inclusions were chosen ore–bearing quartz (4) from stage 3 vein and level 7 in the Wolchon ore body. The ore–bearing quartz is characterized by white–gray color, and therefore samples for the petrology and microthermometric studies are carefully collected from the relatively transparent small quartz crystal (length and width of crystals are 3–5 mm and 0.5–1 mm, respectively, Fig. 4a and b) in pore space of ore veins and polished doubly to thin sections (thickness 0.2–0.4 mm) and fluid inclusions were observed under the microscope to identify their genetic and compositional types, vapor–liquid ratios and the existence of daughter minerals. Microthermometric studies of fluid inclusions were carried out at the laboratory of Faculty of Geology in our University, using Chaixmeca MTM85 heating and freezing stages (from −180 to +600 °C, France). Stage calibration was carried out using synthetic fluid inclusions with standards as CO_2 (–56.6 °C), H_2O (0 °C), naphthalene (80.01 °C), silver nitrate (210 °C), and potassium nitrate (334 °C). The precisions are ± 0.1 °C for temperatures lower than 0 °C, ± 0.5 °C for temperatures of 0–30 °C, and ± 10 °C for temperatures higher than 30 °C. The speed of heating was 5 °C/min and when the phase approached the homogenized state, the speed of heating was decreased, and the homogenization temperature was recorded. The

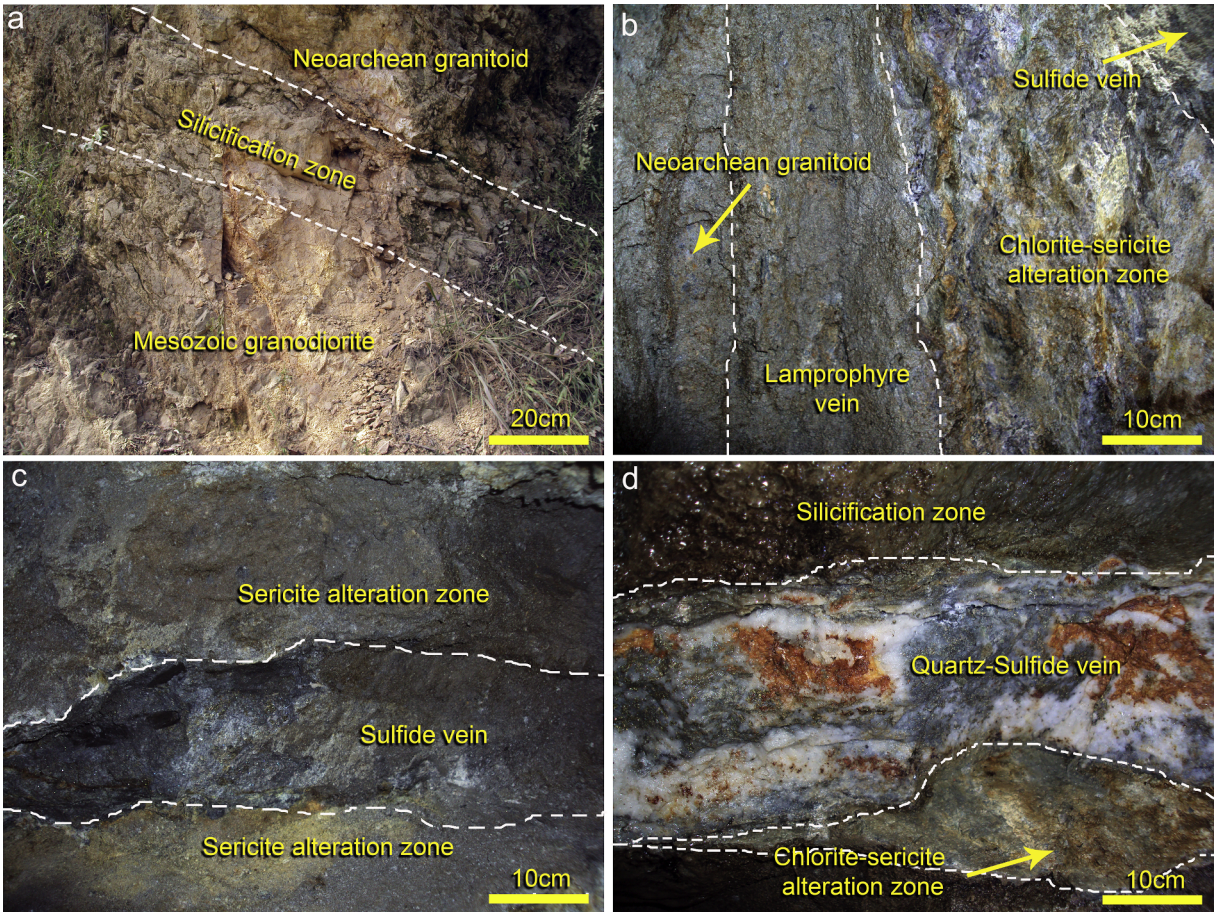

Fig. 3. Photographs of selected alteration zones at Sonchon district. (a) Silicification at the contact of biotite granite and rock of Ryonhwasan Complex. (b, c and d) Alteration zones in the Wolchon ore body (level 7).

freezing temperature was measured by the final melting of ice in inclusions. The liquid nitrogen was used for rapid cooling of the inclusions. The eutectic temperature was measured by method of Roedder (1984). Salinity was calculated using the data of Bodnar (1993), and density was calculated using the data of Brown (1989).

Some white–gray quartz samples from 4 (3), 6 (2), 7 (2) and 10 (4) levels in this ore body were prepared for quantitative determination of group fluid inclusion composition. 100 g of several quartz samples were crushed to 0.3–0.5 mm, then prepared by careful handpicking under a binocular microscope to achieve a purity of > 99%, and were cleaned by following method. The samples and concentrated nitric acid with ratio 1:3 were put into beakers and boiled at the draft chamber for an hour. Then, samples were sorted out and repeatedly cleaned by deionized water and left for one day with deionized water + ion–exchange resin. Dried samples were powdered by an agate mortar with deionized water, and liquid were sorted by centrifugal separator and analyzed by the ICP–MS techniques.

4. Results

4.1. Major elements of the Mesozoic granitoids

Analytical data for the major element compositions of diorite, granodiorite and biotite granite samples are listed in Table 1. All rock samples are relatively fresh as indicated the low LOI values ranging narrowly from 0.23 to 1.98% (Table 1) and by the petrologic observation of unaltered hornblende, biotite and plagioclase.

The diorite has low contents of SiO_2 (55.58–55.88 wt%), Al_2O_3 (14.21–16.55 wt%) and K_2O (1.84–1.93 wt%) and high contents of MgO (5.84–6.77 wt%), Na_2O (3.05–3.27 wt%), Fe_2O_3 (5.32–6.2 wt%), CaO (5.29–6.6 wt%) and P_2O_5 (0.28–0.34 wt%). The granodiorite is characterized by high contents of SiO_2 (60.34–63.56 wt%), Al_2O_3 (16.46–17.76 wt%) and K_2O (2.35–3.43 wt%), and low contents of MgO (2.25–3.39 wt%), and moderate of Na_2O (2.37–4.38 wt%), Fe_2O_3 (3.32–5.02 wt%), CaO (3.21–4.32 wt%) and P_2O_5 (0.25–0.35 wt%). The biotite granite has high contents of SiO_2 (66.15–69.05 wt%), K_2O (3.62–4.82 wt%), and low contents of Al_2O_3 (13.28–15.18 wt%), MgO (0.61–2.31 wt%), Na_2O (2.5–2.7%), Fe_2O_3 (3.25–4.73 wt%), CaO (0.36–0.95 wt%) and moderate of P_2O_5 (0.17–0.23 wt%) (Table1). The diorite has high values of CaO/Na_2O (1.66–2.16) and Na_2O/K_2O (1.69–1.73) ratios, while the values of those for the granodiorite (0.74–1.35 and 0.76–1.41, respectively) and biotite granite (0.14–0.38 and 0.55–0.75, respectively) are low. The values of A/NK and A/CNK ratios are 1.98–2.19 and 0.75–0.91 for diorite, 1.56–2.42 and 1.02–1.36 for granodiorite and 1.40–1.66 and 1.31–1.43 for biotite granite respectively.

4.2. REEs and trace elements

REE and trace element compositions of representative Mesozoic granitoid samples are given in Table 2. REE compositions of wall rocks, ore–bearing and barren quartz samples are listed in Table 3.

Total REE (ΣREE) concentrations range from 218.87 to 229.84 ppm for the diorite, from 214.04 to 226.22 ppm for the granodiorite and from 212.08 to 236.87 ppm for the biotite granite. Chondrite normalized REE patterns indicate that these samples are enriched in the light rare earth elements (LREE) relative to the heavy rare earth elements (HREE), with LREE/HREE ratios of 8.75–8.93, 10.19–11.66 and

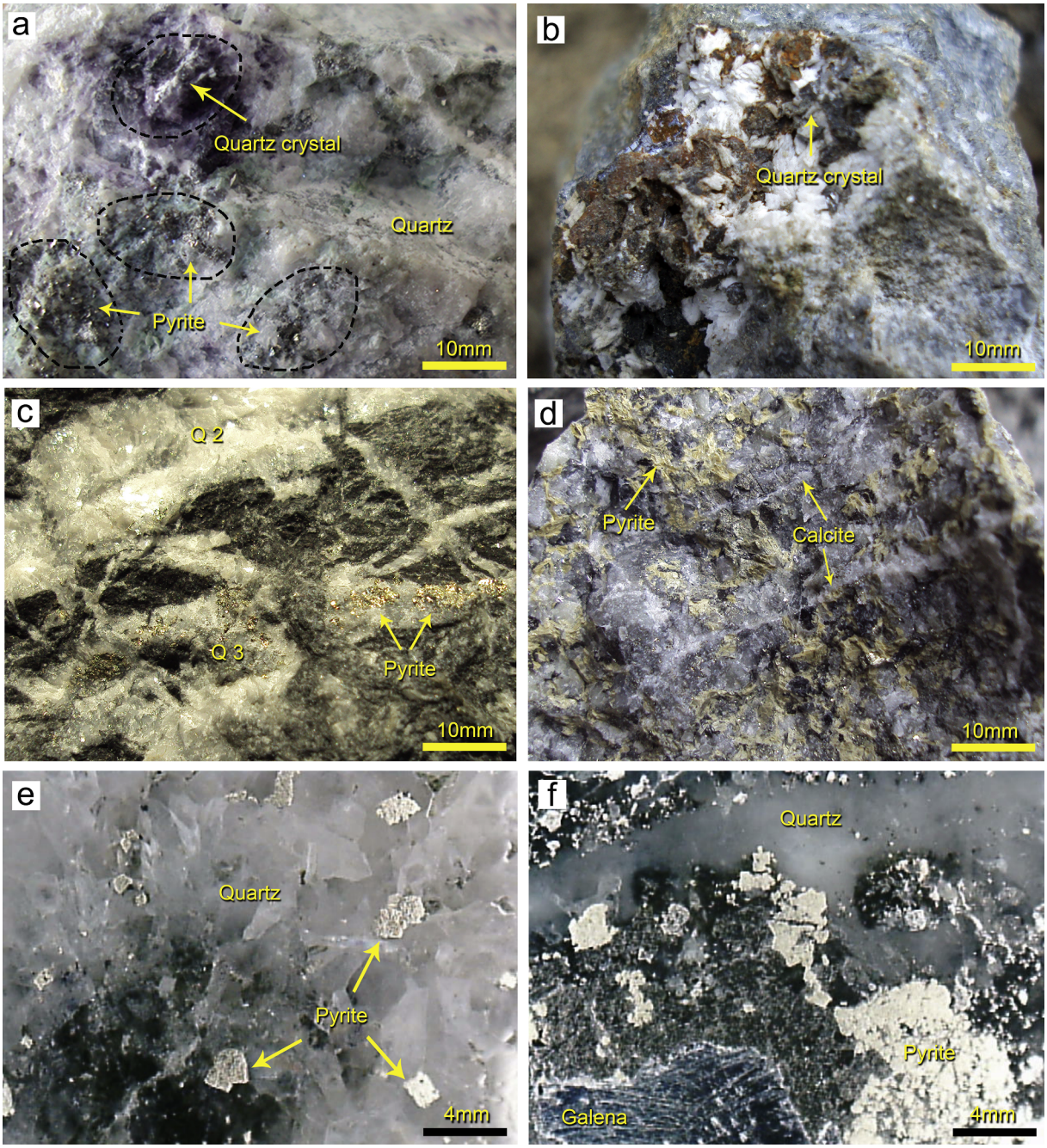

Fig. 4. Photographs of the Wolchon ore body and ores. (a) Quartz in pore space and white quartz with disseminated pyrite. (b) Quartz in pore space. (c) Ore–bearing quartz with pyrite in stage 3 (Q3) and barren quartz in stage 2 (Q2). (d) Pyrite (stage 3) and calcite (stage 4). (e) Euhedral and subhedral pyrite in the Wolchon ore body. (f) Anhedral pyrite and galena in the Wolchon ore body.

8.53–9.03, respectively. They have chondrite–normalized REE distribution patterns that decrease to the right of the diagram (Fig. 11) and negative Eu anomalies (Eu/Eu^* = 0.72–0.86, 0.38–0.40 and 0.41–0.50, respectively) (Table 2). The granitoid have low values of Zr + Nb + Ce + Y (205.36–232.98 ppm for the diorite, 164.97–187.90 ppm for the granodiorite and 152.20–168.70 for the biotite granite). They have high values of Ba (288–756 ppm, 285–578 ppm and 289–396 ppm, respectively) and low values of Sr (152–225 ppm, 125–235 ppm and 125–245 ppm, respectively). The values of Ba/Zr are 4.97–9.44 (diorite), 5.38–25.67 (granodiorite) and 5.56–26.33 (biotite granite), and the values of Sr/Y are 8.96–9.94 (diorite), 7.76–14.48 (granodiorite) and 8.40–8.43 (biotite granite) (Table 2).

The ΣREE concentrations of wall rocks range from 184.42 to 193.12 ppm and are characterized by enrichment in LREE (161.07–171.01 ppm) and depletion in HREE (23.35–22.11 ppm) with LREE/HREE ratios of 6.90–7.73 and have chondrite–normalized REE distribution patterns that increase to the right of the diagram (Fig. 12). These rocks are characterized by negative Eu anomalies (Eu/Eu^* = 0.47–0.56) and are rather smaller than those of the Mesozoic granitoids (Table 3).

In ore–bearing and barren quartz the ΣREE concentrations change from 258.89 to 273.21 ppm and from 199.29 to 237.43 ppm, respectively. They also have clear fractionation between the LREE (240.16–255.01 ppm for the ore–bearing, 180.30–218.50 ppm for the barren) and HREE (18.20–18.73 ppm for the ore–bearing,

Table 1
Major element compositions of Mesozoic granitoids (wt%).

Sample	Diorite			Granodiorite						Biotite granite			
SiO_2	55.67	55.88	55.58	63.56	63.46	61.46	61.06	61.45	60.34	68.5	69.05	68.8	66.15
Al_2O_3	16.55	14.21	15.22	17.61	16.46	16.63	17.1	17.76	17.68	13.28	13.77	13.49	15.18
TiO_2	1.37	1.46	2.39	1.01	2.32	2.41	2.19	2.33	1.68	1.5	1.17	1.37	1.66
Fe_2O_3	5.32	5.54	6.2	3.88	3.32	4.09	4.23	4.43	5.02	3.25	4.5	4.73	4.7
FeO	0.03	0.07	0.06	0.09	0.03	0.05	0.05	0.04	0.06	0.03	0.03	0.04	0.04
MnO	1.07	1.02	1.15	0.99	0.89	0.94	0.92	0.89	0.88	1.66	1.77	1.65	1.79
CaO	6.55	6.6	5.29	4.18	3.58	4.32	3.22	3.21	3.99	0.46	0.52	0.36	0.95
MgO	6.77	6.67	5.84	2.25	2.31	3.24	2.56	3.13	3.39	2.31	0.87	0.61	0.77
K_2O	1.93	1.93	1.84	2.35	3.43	2.37	3.37	3.12	3.17	3.62	4.34	4.82	4.57
Na_2O	3.27	3.05	3.18	3.21	3.44	3.34	4.38	2.37	3.01	2.7	2.5	2.63	2.52
P_2O_5	0.33	0.28	0.34	0.28	0.25	0.29	0.32	0.29	0.35	0.21	0.21	0.17	0.23
LOI	1.41	1.98	1.37	0.56	0.52	0.67	0.51	0.74	0.23	1.3	1.28	1.28	1.25
Total	100.27	98.69	98.46	99.97	100.01	99.81	99.91	99.76	99.8	98.82	100.01	99.95	99.81
$Na_2O + K_2O$	5.2	4.98	5.02	5.56	6.87	5.71	7.75	5.49	6.18	6.32	6.84	7.45	7.09
CaO/Na_2O	2.00	2.16	1.66	1.30	1.04	1.29	0.74	1.35	1.33	0.17	0.21	0.14	0.38
Na_2O/K_2O	1.69	1.58	1.73	1.37	1.00	1.41	1.30	0.76	0.95	0.75	0.58	0.55	0.55
A/NK	2.19	1.98	2.08	2.23	1.74	2.04	1.56	2.42	2.09	1.57	1.55	1.40	1.66
A/CNK	0.86	0.75	0.91	1.15	1.04	1.05	1.02	1.36	1.13	1.43	1.40	1.31	1.40

18.93–18.99 ppm for the barren) with LREE enrichments, LREE/HREE ratios of 12.82–14.01 and 9.49–11.54, respectively. The chondrite–normalized REE distribution patterns of ore–bearing and barren quartz are similar to the Mesozoic granitoids with decreasing to the right of the diagram and negative Eu anomalies (Fig. 12). However, ore–bearing and barren quartz have stronger Eu negative anomalies in comparison with those of Tanchon complex (granitoid) and barren quartz has stronger Eu negative anomalies ($Eu/Eu^* = 0.12–0.13$) than ore–bearing quartz ($Eu/Eu^* = 0.28–0.33$) (Table 3).

4.3. Sulfur isotopes

The sulfur isotopic compositions $\delta^{34}S_{CDT}$ of 19 sulfide minerals as pyrite, sphalerite and galena are listed in Table 4 and the histogram of sulfur isotopic compositions is shown in Fig. 13. The values of $\delta^{34}S_{CDT}$ range from +5.04 to +9.27‰ for pyrite (mean = +7.21‰), from +5.67 to +9.94‰ for sphalerite (mean = +7.81‰) and from +4.80 to +12.46‰ for galena (mean = +8.52‰). On the histogram the values of the $\delta^{34}S_{CDT}$ of sulfides range from +5 to +10‰ (Fig. 13).

Table 2
REE and trace element compositions of Mesozoic granitoids in the study area (ppm).

Sample	Diorite			Granodiorite						Biotite granite			
Pb	30.3	40.1	20.3	20.3	40.3	60.1	40.4	60.3	20.3	60.1	60.1	40.4	60.3
Cd	59.3	28.9	29.3	148.5	59.7	98.6	149.2	19.9	59.9	99.2	140.3	140.8	18.9
Sn	0.9	2.9	2.8	1.9	1.3	2.6	3.1	5.5	3.3	5.1	5.6	3.1	5.5
W	0.1	0.1	0.3	0.3	0.6	0.6	0.3	0.5	0.3	0.1	0.1	0.3	0.5
Cr	82	82	387	198	146	99	48	56	99	57	57	48	58
Ba	765	498	288	578	295	383	385	285	387	396	289	395	289
Sr	211	225	152	135	235	125	155	225	152	235	225	125	245
Nb	14.2	19.5	18.5	18.4	15.1	14.1	9.3	17.3	19.1	20.2	20.5	18.5	19.5
Zr	81	65	58	54	19	45	15	53	18	19	15	15	52
Ta	2.8	2.8	3.2	3.2	4.1	4.5	4.1	3.9	3.8	4.9	5.3	5.5	4.1
La	32.14	30.29		37.39	38.02					50.01	52.37		
Ce	104.24	98.22		88.11	99.64					72.91	89.32		
Pr	12.76	11.16		10.23	10.33					12.01	12.05		
Nd	41.25	39.88		42.37	42.8					37.05	40.13		
Sm	7.57	7.62		8.31	8.89					7.31	8.91		
Eu	1.55	1.89		0.88	0.98					1.22	1.11		
Gd	7.19	7.36		7.62	7.69					9.31	9.36		
Tb	1.98	2.11		1.83	1.71					1.94	1.82		
Dy	9.79	10.1		9.87	8.77					8.46	9.21		
Ho	2.53	2.67		1.21	1.45					2.52	2.62		
Er	4.92	3.88		3.24	3.16					5.01	5.81		
Tm	0.66	0.56		0.48	0.44					0.75	0.74		
Yb	2.89	2.78		2.19	2.07					3.12	3.01		
Lu	0.37	0.35		0.31	0.27					0.46	0.41		
Y	23.54	22.64		17.39	16.23					27.89	26.78		
Zr + Nb + Ce + Y	232.98	205.36		187.90	164.97					152.20	168.70		
HREE	23.14	22.45		19.13	17.87					22.26	23.62		
LREE	206.70	196.42		194.91	208.35					189.82	213.25		
LREE/HREE	8.93	8.75		10.19	11.66					8.53	9.03		
ΣREE	229.84	218.87		214.04	226.22					212.08	236.87		
La/Yb	11.12	10.90		17.07	18.37					16.03	17.40		
Ba/Zr	9.44	7.66	4.97	10.70	15.53	8.51	25.67	5.38	21.50	20.84	19.27	26.33	5.56
Sr/Y	8.96	9.94		7.76	14.48					8.43	8.40		
$(La/Yb)_N$	6.60	6.47		10.14	10.91					9.52	10.33		
Eu/Eu^*	0.72	0.86		0.38	0.40					0.50	0.41		

Table 3
REE compositions of wall rocks, ore–bearing quartz and barren quartz (ppm).

Elements	Wall rocks		Ore–bearing quartz		Barren quartz	
La	30.91	29.32	57.02	66.72	36.2	35.84
Ce	75.32	77.17	111.22	116.2	85.39	112.19
Pr	10.11	10.11	12.8	10.4	10.71	11.37
Nd	27.65	37.06	41.69	44.56	32.75	41.96
Sm	8.13	8.3	9.61	9.21	7.66	8.66
Eu	1.29	1.11	0.69	0.79	0.27	0.31
Gd	7.66	7.94	7.13	7.13	7.32	8.17
Tb	0.82	0.62	0.65	0.78	0.75	0.94
Dy	6.99	7.11	7.81	7.3	6.24	8.41
Ho	2.53	2.69	1.79	2.41	2.23	2.65
Er	5.78	5.04	4.39	4.21	5.3	3.75
Tm	0.95	0.95	0.55	0.52	0.69	0.52
Yb	5.3	4.47	3.19	2.69	3.3	2.31
Lu	0.98	1.23	0.35	0.29	0.48	0.35
Y	51.21	56.12	20.5	16.15	25.3	18.19
HREE	23.35	22.11	18.73	18.20	18.99	18.93
LREE	161.07	171.01	240.16	255.01	180.30	218.50
LREE/HREE	6.90	7.73	12.82	14.01	9.49	11.54
ΣREE	184.42	193.12	258.89	273.21	199.29	237.43
La/Yb	5.83	6.56	17.87	24.80	10.97	15.52
$(La/Yb)_N$	3.46	3.89	10.61	14.73	6.51	9.21
Eu/Eu^*	0.56	0.47	0.28	0.33	0.12	0.13

Table 4
Sulfur isotope compositions of sulfide minerals from the Wolchon ore body.

Number of samples	minerals	$\delta^{34}S$ (‰)
1	Pyrite	5.64
2	Pyrite	9.05
3	Pyrite	6.71
4	Pyrite	7.62
5	Pyrite	7.96
6	Pyrite	8.19
7	Pyrite	6.03
8	Pyrite	7.1
9	Pyrite	5.95
10	Pyrite	8.99
11	Pyrite	5.04
12	Pyrite	9.27
13	Sphalerite	5.67
14	Sphalerite	9.94
15	Galena	4.80
16	Galena	10.6
17	Galena	5.74
18	Galena	8.99
19	Galena	12.46

4.4. Fluid inclusions

4.4.1. Petrology characteristics

Fluid inclusions are common in ore–bearing quartz. Three fluid inclusion types have been identified in quartz: primary, pseudosecondary and secondary. Primary fluid inclusions are only aqueous–rich two–phase with a degree of fill of aqueous phase ranging from 60 to 70% (Fig. 5a–c) at room temperature (25 °C), and have round, ellipsoidal or irregular shapes varying in size from 5 to 10 μm. They occur randomly and are isolated within mineral growth plane and three–dimensional clusters, indicating a primary origin. Pseudosecondary fluid inclusions occur along healed fractures that start in the dark growth zone and extend into the core. They are aqueous–rich inclusions with irregular shapes varying in size from 1 to 10 μm (Fig. 5f). Secondary fluid inclusions are also aqueous–rich two–phase with a degree of fill of aqueous phase ranging from 70 to 80% (Fig. 5d and e), and have oval or irregular shapes varying in size from 2 to 5 μm. They are scattered along healed fractures that start from the crystal surface and extend into the quartz, indicating a secondary origin.

4.4.2. Microthermometry of fluid inclusions

The microthermometric data of primary fluid inclusions in quartz are listed in Table 5. The histogram of homogenization temperatures of fluid inclusions is shown in Fig. 14.

The homogenization temperatures range from 223.5 to 286.3 °C and the melting temperatures of ice range from −0.8 to −2.4 °C. The salinity and the density are 1.39–4.01 wt% NaCl and 0.75–0.85 g/cm^3, respectively.

4.4.3. Composition of aqueous phase of fluid inclusions

The compositions of aqueous phase of fluid inclusions in quartz are listed Table 6. The major ions in aqueous phase are K^+, Na^+, Sb^{3+}, Sn^{4+}, F^-, SO_4^{2-} and Cl^-. The contents of K^+ (0.184–0.579 ppm) increase to low levels, while Na^+ (0.098–0.186 ppm) decrease. The contents of F^- (0.078–0.189 ppm) are high in upper level, in contrast Cl^- (0.332–0.523 ppm) and SO_4^{2-} (15.33–50.18 ppm). The values of X (K^+)/X (Na^+) ratios range from 1.18 to 4.19 and the values of X (F^-)/X (Cl^-) ratios are 0.18–0.36.

5. Discussion

5.1. Major and trace elements of Mesozoic granitoids

Granites are commonly divided into I–, S– or A–types according to the nature of their protolith and their petrographic and geochemical features (Chappell and White, 1974; Loiselle and Wones, 1979). In the study area the Mesozoic granitoids have low Zr + Nb + Ce + Y contents (205.36–232.98 ppm for the diorite, 164.97–187.90 ppm for the granodiorite and 152.20–168.70 ppm for the biotite granite), low Zr contents (mean, 68 ppm, 34 ppm, 25.25 ppm, respectively) and Nb contents (mean, 17.4 ppm, 15.55 ppm, 19.68 ppm, respectively), suggesting I– or S–types (Bonin, 2007; Whalen et al., 1987). The S–type granites are mineralogically characterized by abundant Al–rich minerals, such as muscovite, garnet, cordierite and tourmaline, while I–type granites generally contain amphibole (Zen, 1988; Clemens, 2003). They are strongly peraluminous with A/CNK values > 1.1, while most I–type granites are metaluminous with A/CNK values < 1.0. However, this distinction is not always straightforward because A/CNK values significantly overlap for highly fractionated I- and S–type granites (Chappell, 1999).

In this study, the diorite contains low contents of SiO_2 (55.58–55.88 wt%), whereas the contents of the granodiorite and biotite granite are high (60.34–63.56 wt% and 66.15–69.05 wt%, respectively). In Harker diagram (Figs. 6 and 7), all rocks show similar evolutionary trends with increasing SiO_2 content: Fe_2O_3, TiO_2, Al_2O_3, MgO, Na_2O and CaO contents decrease, except the K_2O content. Diorite and granodiorite are Na–enriched (Na_2O contents are average 3.17 and 3.29 wt%, respectively) in comparison with biotite granite (average Na_2O content of 2.59 wt%). The values of Na_2O/K_2O (average 0.60) for biotite granite display enrichment of K_2O over Na_2O (Na_2O/K_2O < 1), suggesting either crust–derived S–type rocks or assimilation and fractional crystallization processes. Conversely, diorite and granodiorite exhibit the enrichment of Na_2O over K_2O (Na_2O/K_2O average 1.67 and 1.13 respectively), indicating mantle–derived I–type rocks (Esperanca et al., 1992). The diorite exhibits elevated Mg content (average 6.43 wt % MgO) relative to granodiorite (average 2.81 wt% MgO) and biotite granite (average 1.14 wt% MgO), suggesting metaluminous and I–types rocks (Frost et al., 2001). These rocks are alkali–enriched ($K_2O + Na_2O$ = 5.02–7.75 wt%) and classified as high–K calc–alkaline in a K_2O vs. SiO_2 diagram (Fig. 7b). On a $Na_2O + K_2O$ vs. SiO_2 diagram, the granitoid plot in the areas of gabbroic diorite–diorite–granodiorite (Fig. 7c). The diorite has low A/CNK values (0.75–0.91) and plots within the metaluminous field in an A/NK vs. A/CNK diagram, and the granodiorite has medium A/CNK value (1.02–1.36) and plots in weakly peraluminous or peraluminous fields (Fig. 7d). The biotite granite has high A/CNK values (1.31–1.43) and plots in the peraluminous field.

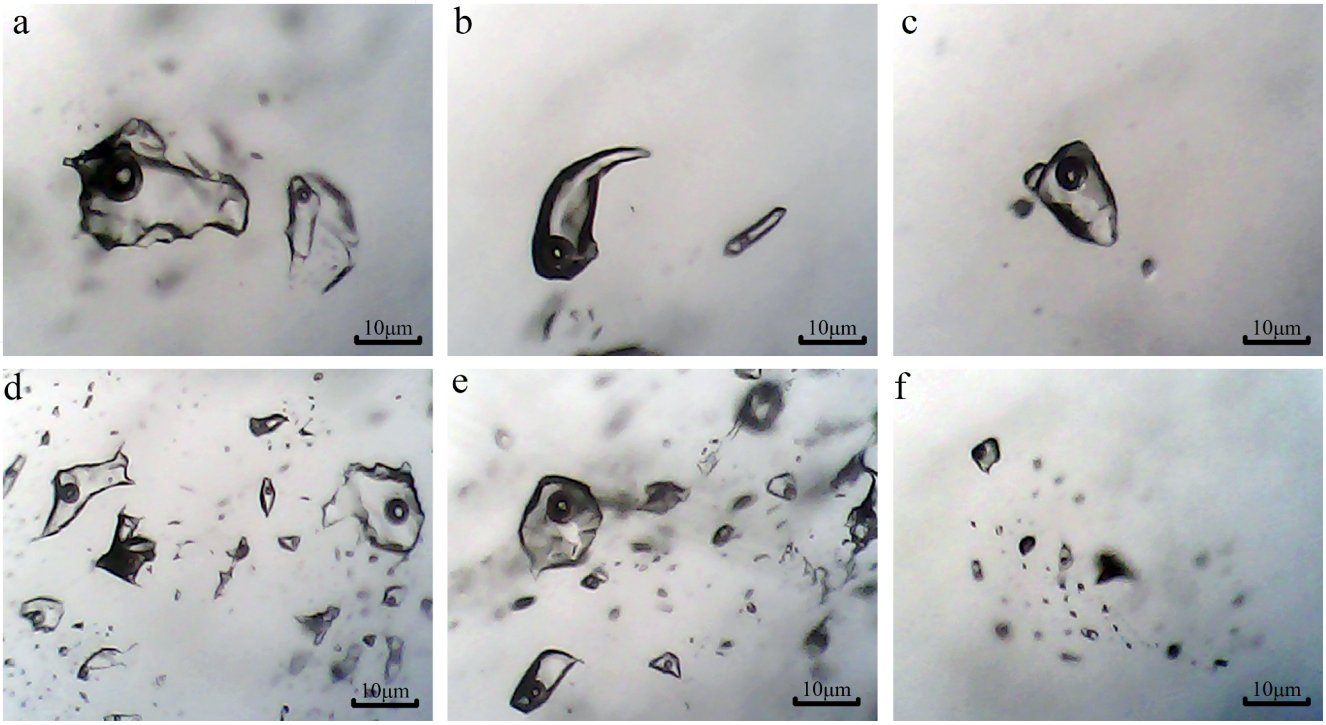

Fig. 5. Primary (a–c), pseudosecondary (f) and secondary (d–e) fluid inclusions in quartz.

Table 5
Microthermometry results of fluid inclusions from the Wolchon ore body.

Level	Eutec.temp./°C	Frees.temp./°C	Homo.temp./°C	Density g/cm^3	Salinity/wt% NaCl
4–1 (6)	−21.4	−1.2	236.3	0.83	2.06
4–2 (12)	−20.6	−1.2	241.3	0.83	2.06
4–3 (4)	−21.2	−0.8	236.3	0.83	1.39
6–1 (2)	−18.9	−1.1	237.1	0.83	1.90
6–2 (11)	−19.5	−0.9	223.5	0.85	1.56
7–1 (3)	−19.9	−0.8	235.3	0.83	1.39
7–2 (1)	−21.5	−1.1	253.3	0.80	1.90
7–3 (3)	−21.8	−1.4	231.1	0.84	2.40
7–4 (1)	−21.3	−1.1	230.6	0.84	1.90
10–1 (1)	−21.2	−1.0	235.4	0.83	1.73
10–2 (3)	−22.3	−1.1	267.3	0.78	1.90
10–3 (3)	−19.8	−1.1	286.3	0.75	1.90
10–4 (8)	−22	−2.4	284.7	0.78	4.01

(The number in brackets is the number of analysis).

Hence, the diorite belongs to I–type, while the granodiorite and biotite granite belong to I–S types and S–types respectively.

P_2O_5 content and the relationship between P_2O_5 and SiO_2 can also be used to determine the magmatic signatures of the granite, primarily by considering the solubility of apatite in different melts and therefore the contrasting behavior of P_2O_5 in I– and S–type granites. P_2O_5 concentrations in I–type granites decrease with increasing SiO_2, as more siliceous melts have lower P solubility. In comparison, P_2O_5 content in S–type granites are either roughly constant or slightly increase with increasing SiO_2 content, suggesting that these magmas never reached P–saturation. Some highly fractionated S–type granites have very high P_2O_5 content (Li et al., 2007; Xiao et al., 2014). In the Mesozoic granitoids of the study area, the negative correlation of the P_2O_5 with increasing SiO_2 displays an I–type trend (Fig. 6f). The samples show high CaO/Na_2O ratios of 1.66–2.16 for the diorite, 0.74–1.35 for the granodiorite, indicating a derivation from clay–poor psammite–derived source, whereas the biotite granite has low CaO/Na_2O ratios of 0.14–0.38, indicating a derivation from clay–rich pelite–derived melt source. On the $Zr + Nb + Ce + Y$ vs. $(K_2O + Na_2O)/CaO$ discrimination diagram by Eby (1992), the diorite belongs to fractionated M–, I–, and S–type granites (FG), while the granodiorite and the biotite granite belong to unfractionated M–, I–, and S–type granites (OGT) (Fig. 10). The plots of $(La/Yb)_N$ – Yb_N (Fig. 8a) and Sr/Y – Y (Fig. 8b) diagrams show that the granitoid are typical arc rocks and have been produced by the partial melting of the lower crust.

5.2. REEs and geological application

The REEs in ore and rocks are effectively applied to clarify the source of ore–forming materials, the evolution of hydrothermal systems, the conditions of wall rock alternation and ore formation, the genesis of ore deposits and the genetic relationship between the ore body and rocks (Henderson, 1984; Lottermoser, 1992; Wang et al., 2016).

The Mesozoic granitic rocks in the study area have similar REE distribution patterns that indicate a relatively uniform and integrated magmatic origin. In detail, they are characterized by LREE (189.82–213.25 ppm) enrichment, HREE (17.87–23.62 ppm) depletion

Table 6
Aqueous Phase composition of fluid inclusions in quartz from the Wolchon ore body (ppm).

Ions	4 (3)	6 (2)	7 (2)	10 (4)
K^+	0.184	0.260	0.579	0.423
Li^+	0.078	0.071	0.089	0.083
Na^+	0.156	0.098	0.186	0.101
Mg^{2+}	0.006	0.006	0.005	0.009
Mn^{2+}	0.003	0.003	0.002	0.004
Ni^{2+}	0.012	0.017	0.011	0.009
Zn^{2+}	0.003	0.003	0.001	0.001
Fe^{2+}	0.065	0.032	0.029	0.074
P^{5+}	0.094	0.081	0.077	0.084
S^{2+}	0.162	0.141	0.098	0.098
Sb^{3+}	0.113	0.169	0.163	0.155
Sn^{4+}	0.181	0.091	0.083	0.086
Ca^{2+}	0.003	0.001	0.001	0.001
F^-	0.189	0.092	0.079	0.078
Cl^-	0.523	0.498	0.332	0.379
SO_4^{2-}	15.33	30.87	38.19	50.18
F^-/Cl^-	0.36	0.18	0.24	0.21
K^+/Na^+	1.18	2.65	3.11	4.19
Na^+/K^+	0.85	0.38	0.32	0.24
Ca^{2+}/Mg^{2+}	0.50	0.17	0.20	0.11

(The number in brackets is the number of samples).

and negative Eu anomalies (Eu/Eu^* = 0.38–0.86), indicating the fractional crystallization of plagioclase or the presence of residual plagioclase in the source of the magmas. In general, Eu anomalies occur mainly in felsic magmas by plagioclase fractionation. The negative Eu anomaly is controlled by the partitioning of Eu into plagioclase during fractionation or the presence of residual plagioclase in the source, and the high oxygen fugacity in the melt can rise to a negative Eu anomaly in REE patterns due to volatile saturation. The total contents of REE (ΣREE) are 218.87–229.84 ppm for the diorite, 214.04–226.22 ppm for the granodiorite and 212.08–236.87 ppm for the biotite granite, respectively. These rocks show a clear fractionation between the LREE and HREE with LREE enrichments, LREE/HREE ratios of 8.53–11.66 and $(La/Yb)_N$ values of 6.47–10.91, and have chondrite–normalized REE distribution patterns that decrease to the right of the diagram, indicating the fairly uniform and not significant differentiation during magmatic evolution (Fig. 11) (Rollinson, 1993a). The plots of La/Sm vs. La (Fig. 9a) and La/Yb vs. La (Fig. 9b) show that a partial melting process plays an important role in generation of granitoid (Zu et al., 2016).

The wall rocks (Neoarchean Ryonhwasan complex) have another REE distribution patterns in contrast with the Mesozoic granitoids. These rocks have also high contents LREE (161.07–171.01 ppm) but lower than those of the granitoids, moderate contents HREE that increases to the right of the diagram and more weakly negative Eu anomalies (Eu/Eu^* = 0.47–0.56) (Fig. 12).

The chondrite–normalized REE distribution patterns in ore–bearing and barren quartz are similar to those of the Mesozoic granitoids. They show a clear fractionation ($(La/Yb)_N$ = 6.51–14.73), with LREE enrichment and HREE depletion in the absence of negative Eu anomalies (Eu/Eu^* = 0.28–0.33 and 0.12–0.13 respectively) and have chondrite–normalized REE distribution patterns that decrease to the right of the diagram (Fig. 12). However, ore–bearing and barren quartz have stronger Eu negative anomalies in comparison with those of the Mesozoic granitoids and wall rocks, indicating a reduction condition due to interaction between hydrothermal fluid and wall rock in ore–forming process or mixing of other fluids. On the other hand, the barren quartz has stronger Eu negative anomalies (Eu/Eu^* = 0.12–0.13) than the ore–bearing quartz (Eu/Eu^* = 0.28–0.33).

5.3. Source of ore forming sulfur

Sulfur provides insights into the origins of sulfide minerals (Rollinson, 1993b). Sulfur in ore–forming fluids can originate from a mantle or magmatic source (0 ± 3‰, Chaussidon and Lorand, 1990), a marine/seawater source (20‰), and reduced sulfur in sedimentary rocks (< 0; Rollinson, 1993b). Most of the magmatic ore deposits have relatively large deviations in $\delta^{34}S$ values from the presumed mantle melt value near zero, indicating magma contamination by interactions with wall rocks (Hoefs, 2015). A magmatic hydrothermal deposit is closely associated in space and time with igneous intrusions that were emplaced at relatively shallow depths. Most of $\delta^{34}S$ values of sulfides fall between −3 and 1‰, whereas those of sulfates fall between +8 and +15‰ (Field and Gustafson, 1976; Shelton and Rye, 1982). Epithermal mineral systems are formed at shallow crustal levels and low temperatures of mineralization (150–350 °C) with variable salinities. There are two possibilities for a magmatic source. Alkalic epithermal deposits have sulfides $\delta^{34}S$ values that vary from −7.9 to +5.5‰ in the early magmatic–hydrothermal system, and from −15 to +8‰ (typically < 0‰) in the epithermal system (Richards, 1995). The isotopic composition of a hydrothermal sulfide is determined by the isotopic composition of the hydrothermal fluid from which the mineral is deposited, the temperature of deposition, the chemical composition of the dissolved element species including pH and fO_2 at the time of mineralization, and the relative amount of the mineral deposited from the fluid (Hoefs, 2015).

In the Sonchon deposit, pyrite, sphalerite and galena are the main sulfides and sulfates are absent in ore bodies, which indicates that the fO_2 of the ore–forming fluid system was low and the sulfur in hydrothermal fluids existed mainly as HS^- and S^{2-}, and that the $\delta^{34}S$ value of pyrite would be close to that of the fluid system (Hoefs, 2004; Ohmoto and Rye, 1979). High values of the $\delta^{34}S_{CDT}$ of pyrite (+5.04–+9.27‰, mean = +7.21‰, n = 12), sphalerite (+5.67–+9.94‰, mean = +7.81‰, n = 2) and galena (+5.74–+12.46‰, mean = +8.52‰, n = 5) are inconsistent with the majority of magmatic hydrothermal deposits (−4 to +3‰). As seen from the histogram of sulfur isotopic compositions (Fig. 13), the $\delta^{34}S_{CDT}$ values are mainly distributed around +5 to +10‰. Based on the previous study, the relatively high values of the $\delta^{34}S$ (from +5.04 to +12.46‰) in sulfides from quartz–gold veins in the Wolchon ore body suggest that the fluid redox state was below the SO_2/H_2S boundary and the dominant reduced sulfur species in the fluids was H_2S (Ohmoto and Rye, 1979). In this state, the $\delta^{34}S$ of sulfide is similar to the $\delta^{34}S$ of fluid (Rollinson, 1993a), i.e., the average $\delta^{34}S$ value of the sulfides can be considered approximately equal to that of the hydrothermal fluids. The positive $\delta^{34}S$ values may be attributed to local reduction of the fluid by fluid–carbonaceous wall rock interaction, or reactions of the hydrothermal fluids with ^{34}S–enriched sulfides in wall rocks (McCuaig and Kerrich, 1998). On the other hand, felsic intrusive rocks have $\delta^{34}S_{CDT}$ values of +0.2–+5.8‰ (Ohmoto and Goldhaber, 1997) and granodiorite has the $\delta^{34}S_{CDT}$ values of −3.6 to +5‰ (Ishihara and Sasaki, 1989) and the $\delta^{34}S$ value of the fluid in equilibrium with granite magma ($\delta^{34}S$ = 0.0‰) is about 5.0‰ (Ohmoto and Rye, 1979). Hence, we suggest that the sulfur within sulfide ores in the Sonchon deposit was derived from a magmatic source. The facts that the carbonaceous rocks are absent in the study area and are present only the sulfides with high $\delta^{34}S_{CDT}$ values in ore body, indicate low fO_2 and high pH of the ore–forming fluid system, and fluid–wall rock interaction or mixing meteoric origin, or dissolution and precipitation of ^{34}S–enriched sulfides in the wall rocks. Based on Ohmoto (1972) and the homogenization temperature (mean 246 °C) of fluid inclusions in this study, the fO_2 conditions during mineralization stage (250 °C) are between −38 and −44 log units and pH is about 10 on the sulfur isotope composition of sphalerite.

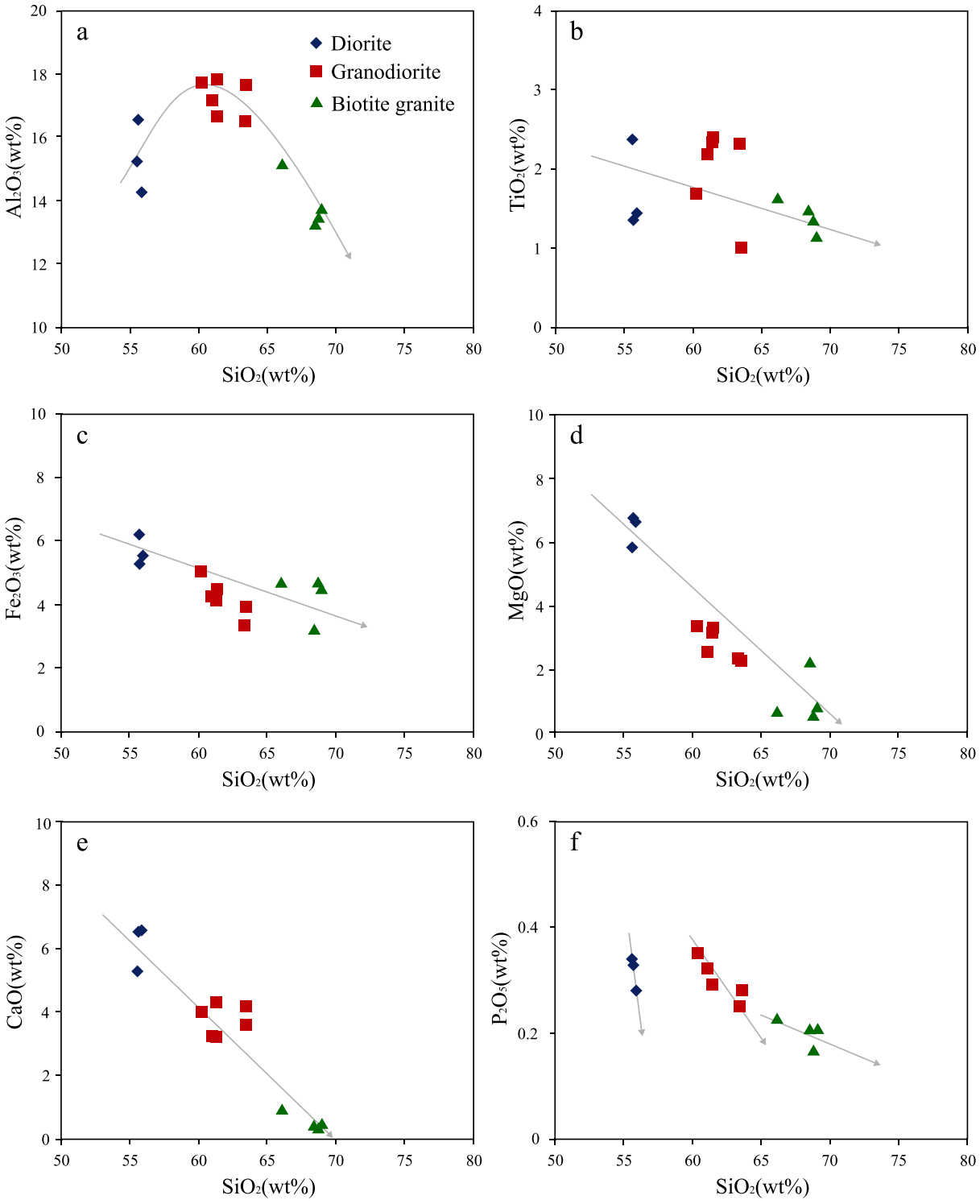

Fig. 6. Chemical variation diagrams for the Mesozoic granitoids in the Sonchon district.

5.4. Nature of fluid inclusions

Primary fluid inclusions in minerals have important aspects to explain the nature of ore–forming fluid and can be used to determine the genesis of the original fluids. The ore–forming fluids of metamorphic origin in many environments hosting gold deposits in the world are H_2O–CO_2 rich with low salinity (Foster, 1989; Peters and Golding, 1989). The molar ratios of aqueous–phase components of fluid inclusions as X (Na^+)/X (K^+) < 2 and X (Na^+)/X $(Ca^{2+} + Mg^{2+})$ > 4 indicate either magma or metamorphic hydrothermal fluid, whereas molar ratios of X (Na^+)/X (K^+) > 2 and X (Na^+)/X $(Ca^{2+} + Mg^{2+})$ < 1.5 indicate hot brine or formation water (Roedder, 1971). A small X (F^-)/X (Cl^-) ratio usually indicates genesis related to underground hot brine or atmospheric precipitation (Lu et al., 1990).

All fluid inclusions in ore–bearing quartz in this study are characterized by only aqueous–vapor phases without CO_2–rich phase and daughter minerals, indicating that ore–forming fluids was homogenous magmatic fluid and had low salinity. The absence of vapor–only or liquid–only primary inclusions in minerals indicates lack of boiling in the hydrothermal system during ore–forming process. The ranges of

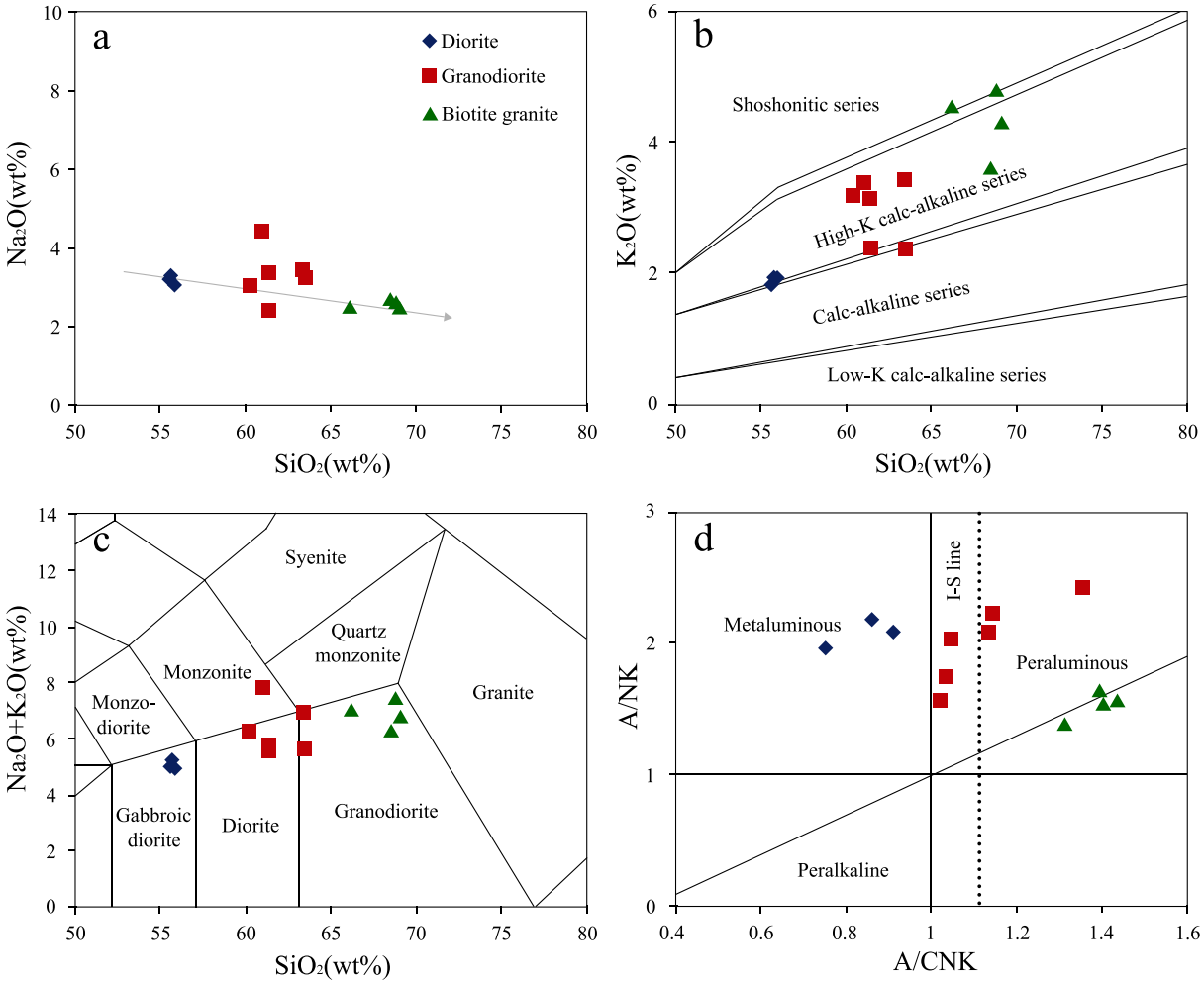

Fig. 7. Na_2O vs. SiO_2 diagram (a); K_2O vs. SiO_2 diagram (b); $K_2O + Na_2O$ vs. SiO_2 diagram (Middlemost, 1994) (c); A/NK vs. A/CNK plot (Maniar and Piccoli, 1989) for the Mesozoic granitoids. A/CNK = $Al_2O_3/(CaO + Na_2O + K_2O)$ molar, A/NK = $Al_2O_3/(Na_2O + K_2O)$ molar.

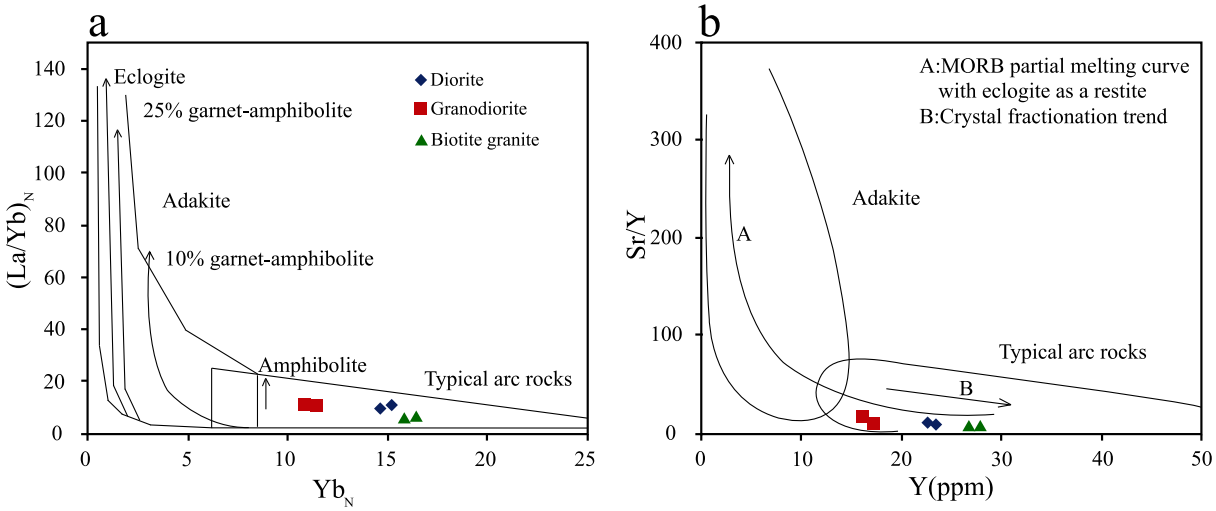

Fig. 8. $(La/Yb)_N$ vs. Yb_N diagram (a) and Sr/Y vs. Y diagram (b) for the Mesozoic granitoids. N means normalized to chondrite (Sun and McDonough, 1989).

measured X (Na^+)/X (K^+) ratios and X (Na^+)/X (Ca^{2+} + Mg^{2+}) ratios are 0.24–0.85 and 10.10–17.33, respectively, indicating magmatic water. On the other hand, low values of X (F^-)/X (Cl^-) ratios (0.18–0.36) indicate underground hot brine or meteoric water (Table 6). Homogenization temperatures of fluid inclusions in ore–bearing quartz range from 223.5 to 286.3 °C with an average of 246 °C (Fig. 14). Final melting temperatures of ice in fluid inclusions vary from −0.8 to −2.4 °C, corresponding to salinities of 1.39 and 4.01 wt% NaCl with an average of 2.01 wt% NaCl. According to the salinity of fluid derived magma (2–10 wt% NaCl) (Hedenquist et al., 1996) and low values of X (F^-)/X (Cl^-) ratios in fluid inclusions in this study, the low salinity of fluid inclusions may be result of magmatic

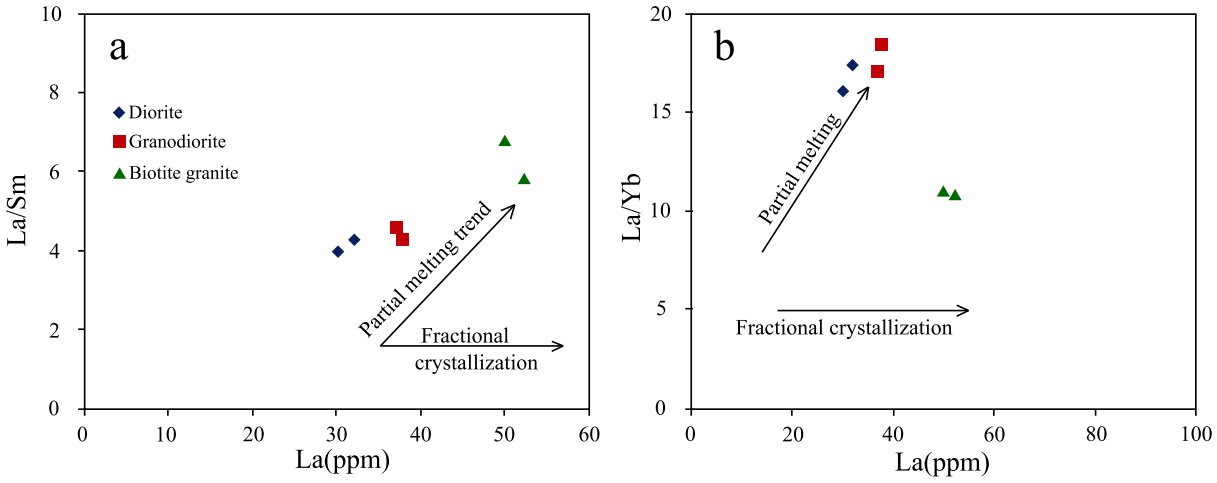

Fig. 9. La/Sm vs. La (a) and La/Yb vs. La (b) of the Mesozoic granitoids (Zu et al. 2016).

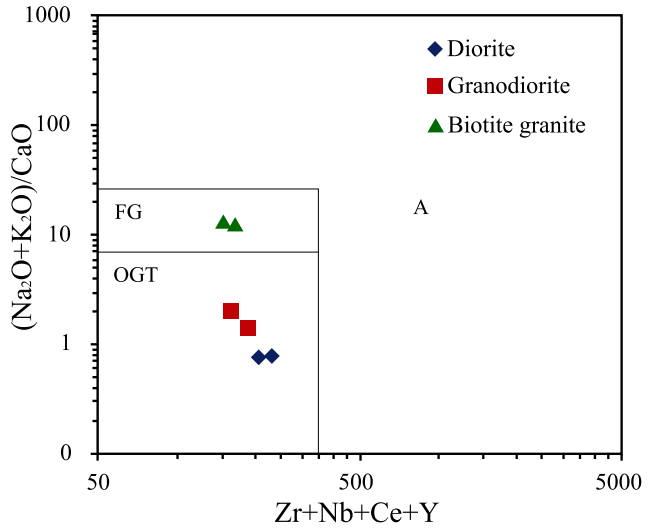

Fig. 10. Zr + Nb + Ce + Y vs. (K_2O + Na_2O)/CaO discrimination diagram for granitoids after Eby (1992). FG – fractionated I–type granitoid; OGT – unfractionated M–, I– and S–type granitoid.

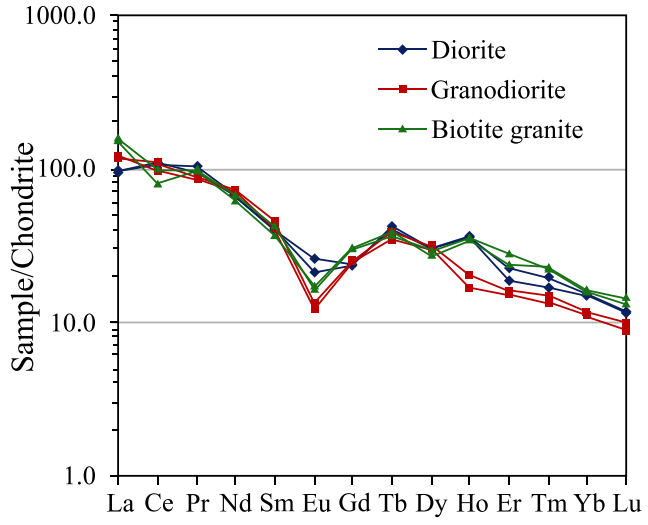

Fig. 11. Chondrite normalized REE of the Mesozoic granitoids in the Sonchon deposit. Chondrite REE values from Sun and McDonough (1989).

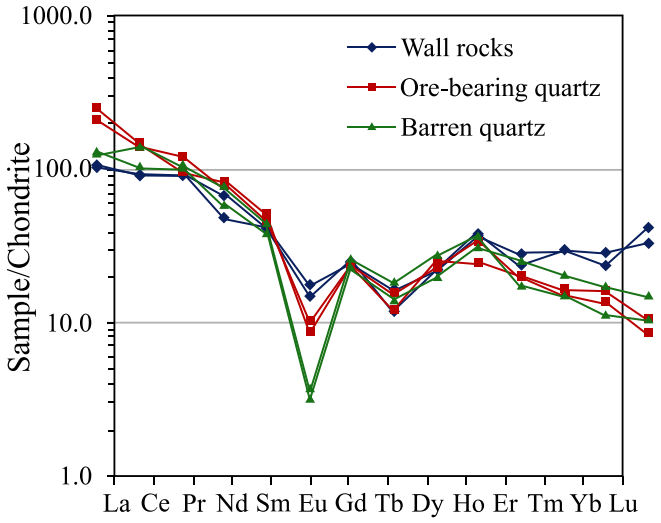

Fig. 12. Chondrite normalized REE of wall rocks, ore–bearing quartz and barren quartz in the Sonchon deposit.

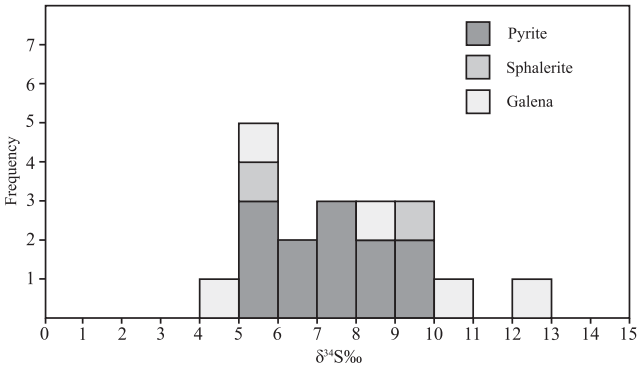

Fig. 13. Histogram of sulfur isotope compositions of sulfide minerals from the Wolchon ore body.

fluid mixing with meteoric. The SO_4^{2-} in solution represents all sulfur–bearing phases in fluid inclusions, such as S^{2-}, HS^- and SO_4^{2-} (Chen et al., 2004), and the high SO_4^{2-} concentration in the ore–forming fluids is also evidence of the existence of magmatic hydrothermal fluid (Jiang et al., 1994). In the fluid inclusions, the contents of SO_4^{2-} are high (15.33–50.18 ppm), indicating genesis related to magmatic water. Hence we suggest that the ore–forming fluid in the

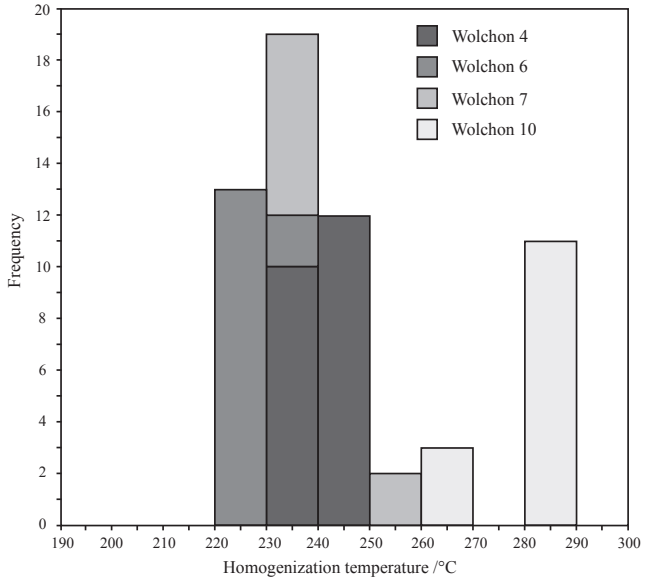

Fig. 14. Histogram of homogenization temperatures of fluid inclusions in quartz.

Sonchon deposit evolved from magmatic fluid mixing with meteoric and had medium temperature and low salinity. According to the eutectic temperatures (−18.9 to −22.3 °C), the fluid inclusions belong to NaCl + H_2O or NaCl + KF + H_2O systems (Roedder, 1984).

6. Conclusions

1) The diorite plots in the metaluminous field in an A/CNK vs. A/NK diagram, while the granodiorite and the biotite granite are weakly peraluminous and peraluminous, respectively. According to chemical composition analysis of Tanchon complex (granitoid), they are typically arc–related rocks, and the diorite and granodiorite were formed by partial melting of clay–poor psammite–derived source, while the biotite granite was derived from clay–rich pelite melt source. The REE distribution patterns indicate a relatively uniform and integrated magmatic origin, and exhibit that a partial melting process plays an important role in their generation. The diorite belongs to I–type, while the granodiorite and biotite granite belong to I–S types and S–types respectively.
2) The sulfur of sulfides in this deposit may come from magma and probably originated from the granodiorite. The ore–forming fluids belong to NaCl + H_2O or NaCl + KF + H_2O and have medium temperature and low salinity, and are homogeneous magmatic hydrothermal fluids that mixed with meteoric water.
3) We have the opinion that the Sonchon deposit is a mesothermal deposit and related to granodiorite. The relationship of the mineralization with granodiorite on the basis of geological evidence described below. First, by the model of metamorphic hydrothermal deposit, it is difficult to explain the fact that all ore bodies in the Sonchon deposit are controlled by faults formed in late Paleozoic and early Mesozoic. Second, ore bodies are hosted only in faults trending NE–SW dipping 70°–80° southeast in the northeastern area of granodiorite, while they do not occur around the diorite and biotite granite. Third, the biotite granite is widely distributed at southwestern and southern parts of Sonchon district without ore bodies and only the fluorite mineralization is present around the diorite. Fourth, the granodiorite is surrounded by hydrothermal alteration, which is infrequent in diorite and biotite granite. Finally, in terms of the REE distribution patterns, the granodiorite and ore–bearing quartz have similar characteristics each other, indicating that the Sonchon mineralization can be closely related to the granodiorite (Fig. 15).

Acknowledgments

We thank the help of the Analytical institutes, pointed in this work and the investigators in the Sonchon Au–polymetallic mines for their help during fieldwork. We are grateful to four reviewers, and Dr. Franco Pirajno for their constructive reviews and significant help in improving the original manuscript. This work was partially supported by the Committee of Education (Grant Number 05–2017), DPR Korea.

Appendix A. Supplementary data

Supplementary data to this article can be found online at https://doi.org/10.1016/j.oregeorev.2018.12.004.

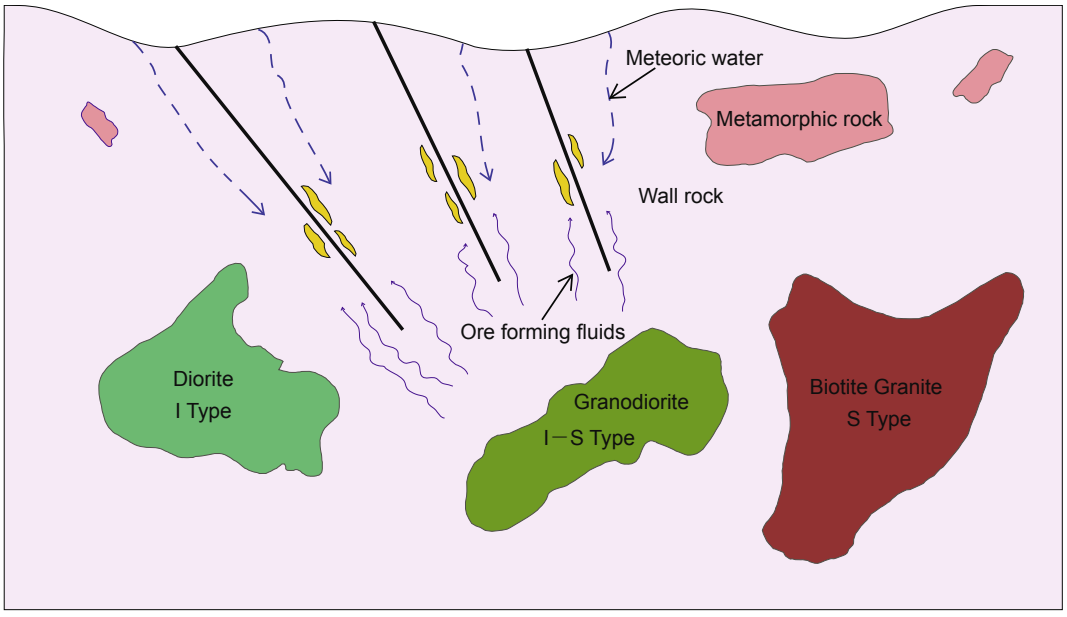

Fig. 15. Metallogenic model for the Sonchon deposit.

References

Barbarin, B., 1999. A review of the relationships between granitoid types, their origins and their geodynamic environments. Lithos 46, 605–626.

Bodnar, R.J., 1993. Revised equation and table for determining the freezing point depression of H_2O–NaCl solutions. Geochim. Cosmochim. Acta 57, 683–684.

Bonin, B., 2007. A–type granites and related rocks: evolution of a concept, problems and prospects. Lithos 97 (1–2), 1–29.

Brown, P.E., 1989. Flincor: a microcomputer program for the reduction and investigation of fluid inclusion data. Am. Mineral. 74, 1390–1393.

Chappell, B.W., 1999. Aluminium saturation in I– and S–type granites and the characterization of fractionated haplogranites. Lithos 46 (3), 535–551.

Chappell, B.W., White, A.J.R., 1974. Two contrasting granite types. Pac. Geol. 8, 173–174.

Chaussidon, M., Lorand, P.J., 1990. Sulphur isotope composition of orogenic spinel lherzolite massifs from Ariege (North–Eastern Pyrenees, France): an ion microprobe study. Geochim. Cosmochim. Acta 54 (10), 2835–2846.

Chen, Y.J., Li, J., Pirajno, F., Lin, Z.J., Wang, H.H., 2004. Diagnostic fluid inclusions of different types gold deposits. Acta Petrol. Sin. 23, 2085–2108 (in Chinese).

Chen, Y.J., Ni, P., Fan, H.R., Pirajno, F., Lai, Y., Su, W.C., Zhang, H., 2007. Diagnostic fluid inclusions of different types hydrothermal gold deposits. Acta Petrol. Sin. 23, 2085–2108 (in Chinese).

Choe, Y.D., Kim, C.S., Choi, B.S., Kim, H.J., Zo, C.H., So, U.R., Li, D.J., Kim, K.C., Kang, S.I., 2011. The Geological Series of Korea (7). Industrial publishing House, Pyongyang, pp. 58–62 (in Korean).

Clemens, J.D., 2003. S–type granitic magmas—petrogenetic issues, models and evidence. Earth Sci. Rev. 61 (1–2), 1–18.

Eby, G.N., 1992. Chemical subdivision of the A–type granitoid: petrogenetic and tectonic implications. Geology 20, 641–644.

Esperanca, S., Crisci, M., de Rosa, R., Mazzuli, R., 1992. The role of the crust in the magmatic evolution of the island Lipari (Aelion Island, Italy). Contrib. Mineral. Petrol. 12, 450–462.

Field, C.W., Gustafson, L.B., 1976. Sulfur isotopes in the porphyry copper deposit at El Salvador, Chile. Econ. Geol. 71, 1533–1548.

Foster, R.P., 1989. Archaean gold mineralization in Zimbabwe: implications for metallogenesis and exploration. Econ. Geol. Monogr. 6, 54–70.

Frost, B.R., Barnes, C.G., Collins, W.J., Argulus, R.J., Ellis, D.J., Frost, C.D., 2001. A geochemical classification for granitic rocks. J. Petrol. 42, 2033–2048.

Groves, D.I., Santosh, M., 2015. Province–scale commonalities of some world–class gold deposits: implications for mineral exploration. Geosci. Front. 6, 389–399.

Han, R.Y., Kim, H., 2005. Geological age of Neoarchean Ryonhwasan Complex (granitoid) by zircon U-Pb dating (ICP-MS). Geol. Geogr. Sci. 1 8–11(in Korean).

Hedenquist, J.W., Izawa, E., Arribas, A., White, N.C., 1996. In: Hydrothermal Systems in Volcanic Arcs, Origin of the Exploration for Epithermal Gold Deposits: A Short Course at Mineral Resource Department. Geological Survey of Japan, Higashi 1–1–3, Tsukuba 305, Japan, pp. 139.

Henderson, P., 1984. General geochemical properties and aboundance of the rare earth elements. In: Henderson, P. (Ed.), Rare Earth Element Geochemistry Developments in Geochemistry 2. Elsevier, Amsterdam, pp. 1–32.

Hoefs, J., 2004. In: Stable Isotope Geochemistry, fifth ed. Springer–Verlag, Berlin, pp. 201.

Hoefs, J., 2015. In: Stable Isotope Geochemistry. Springer, Cham Heidelberg New York Dordrecht London, pp. 389.

Ishihara, S., Sasaki, A., 1989. Sulfur isotope ratios of the magnetite–series and ilmenite-series granitoid of the Sierra Nevada batholith–a reconnaissance study. Geology 17, 788–791.

Jiang, Y.H., Chen, H.N., Wu, Q.H., Chen, S.Z., 1994. Geological characteristics, genesis and further prospecting direction of Ag–Pb–Zn mineralization of Qinxi-Guansi, Zhouning, Fujian. Geophys. Prospect. 30 (4), 21–25 (in Chinese).

Li, J.S., 2009. The genesis of Sonchon gold deposit and prospecting trend in deposit district. J. Geol. Prospect. 2, 13–15 (in Korean).

Li, X.H., Li, W.X., Li, Z.X., 2007. On the genetic classification and tectonic implications of the Early Yanshanian granitoid in the Nanling Range, South China. Chin. Sci. Bull. 52, 1873–1885.

Li, Y.I., 1998. The genesis of Shonchon deposit. J. Geol. Prospect. 4, 10–15 (in Korean).

Loiselle, M.C., Wones, D.R., 1979. Characteristics and origin of anorogenic granites. In: Abstracts of Papers to be Presented at the Annual Meetings of the Geological Society of America and Associated Societies, San Diego, California, November 5–8 11, p. 468.

Lottermoser, B.G., 1992. Rare earth elements and hydrothermal ore formation processes. Ore Geol. Rev. 7, 25.

Lu, H.Z., Li, B.L., Shen, K., Zhao, X.H., Yu, T.J., Wei, J.X., 1990. In: Geochemistry of Fluid Inclusion. Geological Publishing House, Beijing, pp. 153–154 (in Chinese).

Maniar, P.D., Piccoli, P.M., 1989. Tectonic discrimination of granitoids. Geol. Soc. Am. Bull. 101 (5), 635–643.

McCuaig, T.C., Kerrich, R., 1998. P-T–t–deformation–fluid characteristics of lode gold deposits: evidence from alteration systematics. Ore Geol. Rev. 12, 381–453.

Middlemost, E.A., 1994. Naming materials in the magma/igneous rock system. Earth Sci. Rev. 37 (3), 215–224.

Ohmoto, H., 1972. Systematic of sulfur and carbon isotopes in hydrothermal ore deposits. Econ. Geol. 7 (5), 551–578.

Ohmoto, H., Goldhaber, M.B., 1997. Sulfur and carbon isotopes. In: Barnes, H.L. (Ed.), Geochemistry of Hydrothermal Ore Deposits, third ed. John Wiley & Sons Inc., New York, pp. 517–611.

Ohmoto, H., Rye, R.O., 1979. Isotopes of sulfur and carbon. In: Barnes, H.L. (Ed.), Geochemistry of Hydrothermal Ore Deposits, second ed. Wiley, New York, pp. 509–567.

Paek, R.J., Kan, H.G., Jon, G.P., Kim, Y.M., Kim, Y.H., 1993. In: Geology of Korea: Geological Institute Academy of Sciences of DPR Korea. Foreign Languages Books Publishing House, pp. 610.

Peters, S.G., Golding, S.D., 1989. Geologic, fluid inclusion and stable isotope studies of granitoid–hosted gold–bearing quartz veins, Charters Towers, Northeastern Australia. Econ. Geol. Monogr. 6, 260–273.

Richards, J.P., 1995. Alkalic–type epithermal gold deposits–a review. Mineral. Assoc. Can. Short Course Ser. 23, 367–400.

Roedder, E., 1971. Fluid inclusions studies on the porphyry–type ore deposits at Bingham, Utah, Butte, Montana, and Climax, Colorado. Econ. Geol. 66 (1), 98–120.

Roedder, E., 1984. Fluid Inclusions: Reviews in Mineralogy v. 12, 644.

Rollinson, H.R., 1993a. In: Discriminating Between Tectonic Environments using Geochemical Data. Using Geochemical Data: Evaluation, Presentation, Interpretation. Longman Scientific & Technical, Essex, UK, pp. 171–214.

Rollinson, H.R., 1993b. In: Using Geochemical Data: Evaluation, Presentation, Interpretation. Longman Sci. Technol. Press, pp. 306–308.

Shelton, K.L., Rye, D.M., 1982. Sulfur isotopic compositions of ores from Mines Gaspe, Quebec: an example of sulfate–sulfide isotopic disequilibria in ore forming fluids with applications to other porphyry type deposits. Econ. Geol. 77, 1688–1709.

Sun, S.S., McDonough, W.F., 1989. Chemical and isotopic systematics of oceanic basalts: implications for mantle composition and processes. In: In: Saunders, A.D., Norry, M.J. (Eds.), Magmatism in Ocean Basins, vol. 42. Geological Society of Special Publication, London, pp. 313–345.

Wang, Y.B., Zeng, Q.D., Zhou, L.L., Chu, S.X., Guo, Y.P., 2016. The sources of ore–forming material in the low–sulfidation epithermal Wulaga gold deposit, NE China: Constraints from S, Pb isotopes and REE pattern. Ore Geol. Rev. 76, 140–151.

Whalen, J.B., Currie, K.L., Chappell, B.W., 1987. A–type granites: geochemical characteristics, discrimination and petrogenesis. Contrib. Mineral. Petrol. 95 (4), 407–419.

Xiao, B., Li, Q.G., Liu, S.W., Wang, Z.Q., Yang, P.T., Chen, J.L., Xu, X.Y., 2014. Highly fractionated Late Triassic I–type granites and related molybdenum mineralization in the Qinling orogenic belt: Geochemical and U-Pb–Hf and Re–Os isotope constraints. Ore Geol. Rev. 56, 220–233.

Zen, E.-A., 1988. Phase relationships of peraluminous granitic rocks and their petrogenetic implications. Annu. Rev. Earth Planet. Sci. 16, 21–51.

Zhu, D.C., Zhao, Z.D., Niu, Y.L., Dilek, Y., Hou, Z.Q., Mo, X.X., 2013. The origin and preCenozoic evolution of the Tibetan Plateau. Gondwana Res. 23, 1429–1454.

Zu, B., Xue, C.J., Chi, G.X., Zhao, X.B., Li, C., Zhao, Y., Yalikun, Y., Zhang, G.Z., Zhao, Y., 2016. Geology, geochronology and geochemistry of granitic intrusions and the related ores at the Hongshan Cu–polymetallic deposit: Insights into the Late Cretaceous post–collisional porphyry–related mineralization systems in the southern Yidun arc, SW China. Ore Geol. Rev. 77, 25–42.